applied sciences

MDPI

Article

Composition-Dependent Structural Integrity of $Hf_6Ta_2O_{17}$ Superstructure during Sintering in a Reducing Atmosphere

Sang-chae Jeon

School of Materials Science and Engineering, Changwon National University, 20, Changwondaehak-ro, Uichang-gu, Changwon, Gyeongsangnam 51140, Korea; scjeon@changwon.ac.kr; Tel.: +82-55-213-3718; Fax: +82-55-213-6486

Received: 20 May 2020; Accepted: 1 June 2020; Published: 2 June 2020

Abstract: The applicability of a $Hf_6Ta_2O_{17}$ superstructure to a sintering crucible in pyroprocessing was evaluated herein. Samples were prepared by simple oxidation of casted Hf-Ta alloys containing different Ta contents (20.2, 27.2, and 35.2 in at. %). The physical integrity of the oxidized samples was tested after passivation, which resulted in the formation of a $Hf_6Ta_2O_{17}$ superstructure. As a result, only the sample with the lowest Ta content (20.2 at. %) was intact while others were destroyed by peeling off. Based on the XRD analysis, this originates from reduction of the Ta oxide phase from Ta_2O_5 to $Ta2O_{2.2}$, which may lead to severe stresses due to changes in the crystal structure and lattice constant. It is therefore concluded that the Ta content should be lowered within a range permitting the formation of $Hf_6Ta_2O_{17}$. This provides practical data for a beneficial composition design that can be extended to other applications prepared under reducing atmospheres.

Keywords: pyroprocessing; head-end; crucible; $Hf_6Ta_2O_{17}$; oxidation resistance; reduction resistance

1. Introduction

Since its first development in the 1960s in the U.S. as a promising solution to problems regarding accumulated spent fuel, pyroprocessing, which recycles spent fuel as a fuel material and reduces the amount and toxicity of the spent fuel, has also been studied at KAERI (Korea Atomic Energy Research Institute) [1–4]. Pyroprocessing begins with the head-end process, which recovers fuel oxide from the spent fuel and converts it into the form of a UO_2 porous pellet. As a starting process of the pyroprocessing, the head-end consists of sequential subprocesses: de-cladding, mixing, pelletizing, and sintering [5–8].

As noted in a previous paper [9], a reduction process has been adopted between the pelletizing and sintering processes to protect metallic crucibles from oxidation attack during sintering. Molybdenum has been used as the metallic crucible material due to its excellent chemical and physical integrity, in addition to its outstanding thermal shock resistance up to high temperature. However, unless reduction heat treatment is preceded, the metallic crucible will be oxidized during sintering. The uranium oxide in the form of UO_{2+x} gives off oxygen accompanied by a reduction to the UO_2 phase during sintering in a reducing atmosphere. The oxygen forms an oxidative atmosphere temporarily in the vicinity of the pellets and thus attacks the metallic crucible, even under the reducing atmosphere [9]. To inhibit this oxidation attack, U_3O_8 pellets are pre-reduced to UO_2 by high-temperature heat treatment to eliminate the oxygen source before sintering. This allows the use of a commercial metallic sintering crucible without any other treatment. In other words, without an appropriate alternative material for the sintering crucible, reduction heat treatment is inevitably required.

However, such heat treatment requires high temperature, ~1000 °C [9], and a long processing time, detrimentally affecting processing economics and safety. Therefore, once a successful alternative

material is developed for the crucible, the reduction process should be excluded. Requirements for the alternative material are very strict: it should possess oxidation and reduction resistance, as well as excellent thermal shock resistance up to high temperature. This is why studies for the development of an alternative crucible material should be carried out in parallel to related research. Modifications of existing materials, such as surface coatings, may be promising routes. As a general approach, a coating of a promising material satisfying the requirements for a metallic crucible could be a possibility. However, it would be strictly limited when the scale is enlarged under a severe temperature gradient [10]. In addition, if the shape of the coated material is irregular or complex, the coating method will hardly form a uniform passivation layer over the surface. Unfortunately, the sintering crucible in pyroprocessing presents difficulties in terms of size and shape. To meet processing yield requirements, the size of the crucible reaches about 300 mm in diameter [9], and penetration holes facilitating the flow of atmospheric gas should be made in its bottom surface. In other words, a promising method of surface passivation of the metallic crucible is required to overcome the problems related to size and shape.

Previous studies highlighted the formation of an oxidation-resistant $Hf_6Ta_2O_{17}$ superstructure in Hf-Ta alloy systems as a favorable method for passivation [11,12]. Basically, the Hf-Ta alloys have sufficiently higher melting temperature, ~2000 °C, than the sintering temperature used in pyroprocessing, ~1450 °C. Moreover, a uniform oxide can be formed because its formation is due to solid/vapor reaction-induced oxidation of the metallic surface. By securing solid/vapor contact, a uniform superstructure layer can be formed even on the inner surface of penetration holes. In addition, the oxide is known for its excellent oxidation resistance up to high temperature with excellent adhesion, and it is referred to as a superstructure [12]. If the superstructure is confirmed to be reduction resistant and to maintain physical integrity under the sintering conditions in pyroprocessing, it will be appropriate for sintering crucibles. This study confirms the uniform formation of the superstructure and evaluates its applicability by a thermal test with the same sintering conditions as those used in the head-end process in pyroprocessing. To this end, a direction of compositional design is suggested based on the experimental results to enhance the usefulness of the superstructure.

2. Experimental

Commercial metal granules of Hf (99.95% purity, Alfa Aesar) and Ta (99.95% purity, Alfa Aesar) were used as raw materials for the preparation of Hf-Ta alloys with different compositions. The atomic fraction of Ta in the Hf-Ta alloy was varied in a specific range in which it is known to form the $Hf_6Ta_2O_{17}$ superstructure [12]: Hf-xTa (x = 20.2, 27.2, 35.2 in at. %; hereafter, the compositions are denoted in at. % unless otherwise stated). In order of increasing Ta content, the three kinds of samples are denoted hereafter as HT-1, HT-2, and HT-3, as summarized in Table 1. The proportioned granules were alloyed by arc melting into ingots. In order to prevent chemical homogeneity, each ingot was flipped over several times (more than five times) during the arc melting. Ingots obtained from the arc melting were sliced into several mm sizes. The surface was polished using diamond suspensions, finishing at 1 micron.

Table 1. Chemical compositions of the Hf-Ta alloy samples.

Sample	Ta % in Hf-Ta Alloy		Ref. [12] (at. %)
	(wt. %)	(at. %)	
HT-1	20.2	19.8	19.7 *
HT-2	27.8	27.2	26.7 *
HT-3	36.3	35.2	34.7

* $Hf_6Ta_2O_{17}$ superstructure.

For the oxidation, the Hf-Ta alloy ingots were heat treated at 1500 °C for 10 min in laboratory air, resulting in the $Hf_6Ta_2O_{17}$ superstructures according to a previous study [12]. The crystal structure of the Hf-xTa alloy samples was examined using X-ray diffraction (XRD, Rigaku Mini-Flex, Rigaku, Japan) before and after the oxidation treatment. The diffraction patterns of the samples were identified using MDI Jade 6 (Materials Data, Inc. Liverpool, CA). The microstructures of the samples were observed by scanning electron microscopy (SEM, Philips XL-30, Eindhoven, The Netherlands) and energy-dispersed X-ray spectroscopy equipped with SEM. For the purpose of this study, the Hf-Ta alloys with the $Hf_6Ta_2O_{17}$ superstructures were examined in terms of whether they endured the sintering conditions in the head-end process for pyroprocessing. Therefore, the oxidized alloy samples were heat treated under the same conditions for 1 h at 700 °C and then for 24 h at 1450 °C in 4% H_2-Ar atmosphere. After repeated heat treatment, the residual samples were analyzed by XRD, SEM, and EDS.

3. Results and Discussion

Figure 1 shows the XRD patterns of the as-cast ingot samples with different chemical composition, as listed in Table 1. The HT-1 and HT-2 samples containing relatively higher Hf (lower Ta) content were revealed as mixtures of the hexagonal close-packed (HCP) α-Hf and body-centered cubic (BCC) Hf-Ta phases. Except for a peculiar peak observed near 65°, the HT-1 sample showed the same tendency as the HT-2 sample. On the other hand, in the case of the HT-3 sample, no peak of the HCP (α-Hf) phase was observed and only the BCC (Hf-Ta) phase was identified. Despite incomplete identification due to the unknown peaks, it is clearly shown that a phase transition occurred between the HT-2 and HT-3 samples. The same tendency was also observed in a previous paper: constituent phases changed from a mixture of both α-Hf and Hf-Ta into Hf-Ta phase alone with increasing Ta content from 19.7 to 26.7 [12]. Meanwhile, the critical chemical composition leading to phase transition appears to lie between 27.2 and 35.2 (% Ta) in this experiment, considering the chemical compositions of the HT-2 and HT-3 samples. This discrepancy can be attributed to a locally different chemical composition that arises during the arc melting process, even when the cross section appears to be uniform without an unmelted phase, as shown in the inset photograph in Figure 1. Nevertheless, the well-known $Hf_6Ta_2O_{17}$ phase as a superstructure was expected from the HT-2 and HT-3 samples because its formation range is known to be sufficiently broad in terms of chemical composition [12]. To form the superstructure, the same method of oxidation was applied.

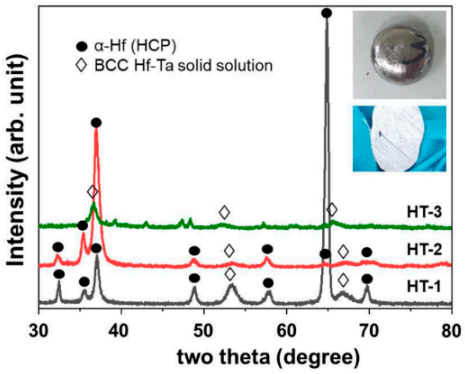

Figure 1. XRD spectra of as-cast ingots with different composition.

Figure 2 shows the SEM and EDS results on a cross section of the HT-1 sample after oxidation heat treatment. The cross-sectional images reveal the outermost layer (surface layer), which is distinguished by its contrast from the substrate region. In a low-magnification micrograph, the thickness of the surface layer appears to be quite uniform along the surface. In both SEM images in Figure 2, the position of the interface between the substrate and surface layer is denoted by dashed lines. Taking into account the applicability of this oxidized alloy as a crucible material in pyroprocessing, the uniformity

provides practical benefits. This is attributed to the even diffusion depth of oxygen by the solid/vapor reaction from the surface. As long as solid/vapor contact is secured between the alloy and gaseous oxygen, the oxide scale can be formed uniformly regardless of the shape of the sample. This gives practical significance where other well-known passivation coating methods are not effective due to the irregular shape of the materials to be passivated.

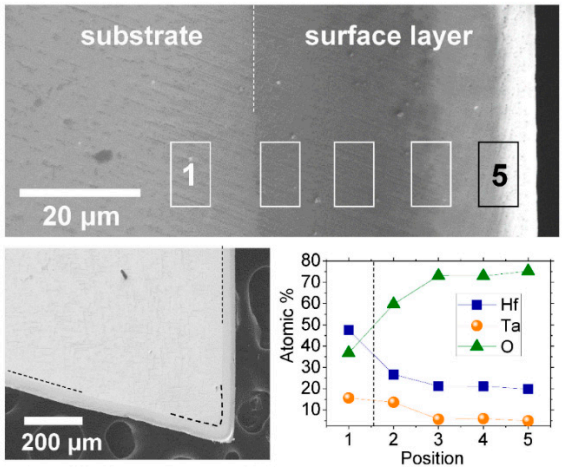

Figure 2. SEM and EDS results on the reaction layer of the HT-1 sample after oxidation. The dashed lines indicate the interface between the substrate and surface layer formed during oxidation.

Across the well-defined interface between the substrate and surface layer, an EDS scan was carried out, as shown in Figure 2. It provides the compositional distribution of Hf, Ta, and O across the interface. To minimize any local fluctuation that may result from local heterogeneity, the EDS signal was collected from a specific area. As a result, every element shows typical diffusional profiles: the oxygen content drastically increased and then became saturated near the surface, while both Hf and Ta gradually decreased and then became saturated towards the surface layer.

The newly formed oxide scale was examined more precisely from the HT-3 sample by SEM and EDS, as shown in Figure 3. The HT-3 sample, containing a relatively high amount of Ta, revealed a thicker layer than did the other samples with a lower amount of Ta. Despite the edge effect of SEM (abnormally bright contrast), the micrographs with higher magnifications clarify two different layers distinguished by their morphology. The inner layer in the vicinity of the substrate reveals a heterogeneous phase, while the outer layer appears as a uniform phase. The regions near the interface between the substrate and the inner layer and that between the inner and outer layers (denoted by "A" and "B", respectively) are enlarged in Figure 3. In addition, the spatial compositional distribution was revealed by EDS mapping at interface "A". At both "A" and "B", relatively higher Ta content was observed from the irregular shape with bright contrast. On the other hand, the dark phase contained a larger amount of Hf than Ta. Considering the morphology and the compositional distribution together with the previous analysis results [12], the inner layer is regarded as a "reaction layer", which is composed of hafnium oxides and β-Ta(Hf) phases, whereas the outer layer is an "oxide layer" of $Hf_6Ta_2O_{17}$ superstructure. An EDS point scan revealed the local composition of the hafnium oxides to be 28.58Hf-3.21Ta-68.21O, that of β-Ta(Hf) to be 19.57Hf-33.93Ta-46.50O, and that of the $Hf_6Ta_2O_{17}$ superstructure to be 22.85Hf-7.08Ta-70.07O. It is noted that the atomic ratio of the oxide layer closely matches the previous observation [12]. In the reaction layer, from the area near the substrate to the oxide layer, the size of the β-Ta(Hf) phase and its connectivity decreased simultaneously. Thus, the Ta content gradually decreased outwards, resulting in the compositional profile shown in Figure 2. However, the chemical composition was similar regardless of the position; i.e., a similar composition was observed at the "A" interface to that at the "B" interface. All these observations are quite similar to those in a previous study that revealed the same β-Ta(Hf) phase in the reaction layer by XRD [12].

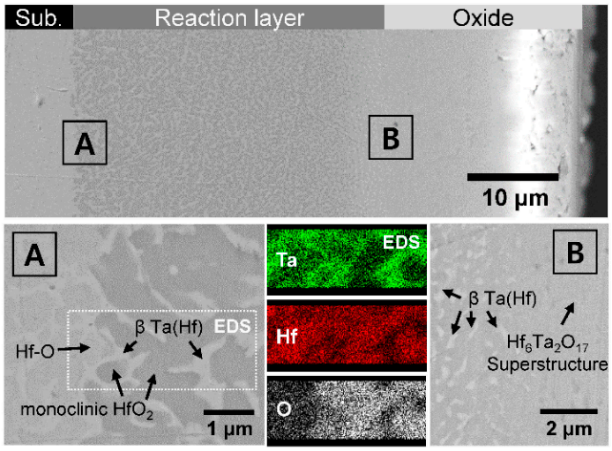

Figure 3. SEM and EDS results on the reaction layer of the HT-3 sample after oxidation.

Figure 4 shows the thermal profile of the sintering process in the head-end of pyroprocessing [8], where it is speculated that the $Hf_6Ta_2O_{17}$ superstructure can be applied as a crucible material. The crucible material should endure both oxidative and reducing atmospheres during repeated thermal cycles. At the initial stage, during ramping, the uranium oxide contained in a crucible starts to be reduced, giving off oxygen gases resulting in the oxidation of metallic crucibles. Reduction of U_3O_8 in a 4% H_2-Ar balanced atmosphere is known to start and finish at about 500 °C and 900 °C, respectively [9]. During ramping through this temperature range, the crucible material must remain intact against the oxidation attack. The oxygen generated from the reduction of uranium oxide creates a locally oxidative atmosphere despite abundant hydrogen gas in the atmosphere. Although the oxidation attack would initially focus on the surface, it can be widespread, and moreover, the degree of damage would be severe as the processing scale is enlarged [9]. Consequently, during the initial stage of sintering (denoted as "O_2(g) emit" in Figure 4), the crucible material should be oxidation resistant. Soon after, the crucible material is surrounded by a H_2-containing reducing atmosphere, and it should endure the reducing attack up to 1450 °C, which is the highest temperature during sintering in the head-end process. From a thermodynamic viewpoint, the oxygen partial pressure (P_{O_2}) increases as the temperature increases; thus, the reduction attack rate would be mitigated, whereas its kinetics can be thermally stimulated.

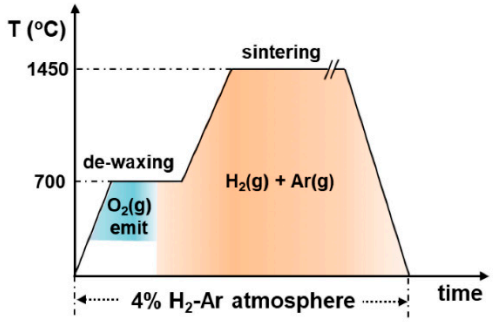

Figure 4. Thermal profile of the sintering process in the head-end of pyroprocessing.

A candidate material for the crucible should thus be reduction resistant in addition to being oxidation resistant.

Figure 5 shows SEM micrographs of the HT-1 and HT-3 samples after the thermal cycle shown in Figure 4. From both macroscopic- and microscopic-scale observations, consistent results were obtained. In the HT-1 sample, the surface layer shown in Figure 2 (reaction layer + oxide layer) was intact with a sharp edge line, while a rough surface layer was observed in the HT-3 sample. In a high-magnification

observation of the HT-3 sample, the outermost surface layer appears to have peeled off partially or mostly (indicated by an arrow in Figure 5b). However, the interfaces between the substrates and reaction layers were maintained as straight lines in all samples, suggesting that the thermal treatment hardly gives rise to additional oxygen diffusion into the substrates. In other words, oxidative attack during ramping was negligible in the $Hf_6Ta_2O_{17}$ superstructure sample.

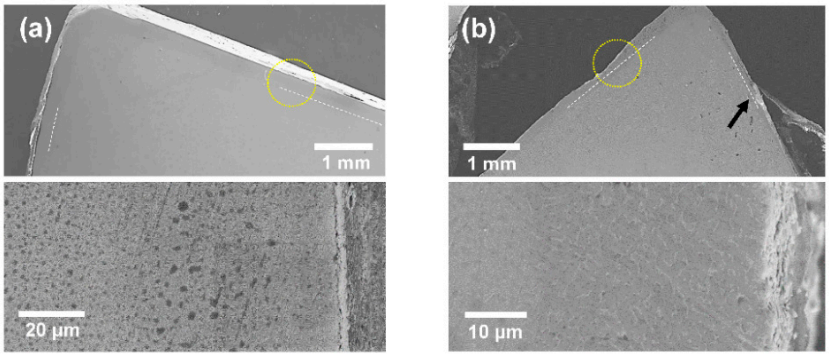

Figure 5. SEM micrographs of the (**a**) HT-1 and (**b**) HT-3 samples after heat treatment in a 4% H_2-Ar atmosphere.

To clarify the cause of the different peeling behaviors among the samples with different Ta contents, the chemical composition was observed by SEM/EDS at the samples' surface regions. Figure 6 shows the SEM/EDS line scan results on the cross-sectional surfaces of the HT-1 and HT-3 samples after the thermal cycle. The average atomic ratios of the constituent elements were measured as 18.6Hf–8.2Ta–74.2O for the HT-1 sample and as 27.2Hf–8.1Ta–64.7O for the HT-3 sample in the vicinity of the surface. However, the measured region was different depending on whether or not the sample surface was conserved after the thermal cycle. The chemical composition could be examined at the outermost oxide layer only in the HT-1 sample with no severe peeling. In contrast, the EDS results for the HT-3 sample show the chemical composition near the interface between the substrate and the reaction layer. According to the position, the atomic ratios in the HT-1 and HT-3 samples are similar to those at Position 5 and at Position 2 in the EDS results shown in Figure 2. Therefore, no evidence for the cause of the surface peeling behavior was drawn from the EDS measurements. Meanwhile, the atomic ratio of Ta slightly increased in both samples compared to that in the sample before the thermal cycle. This is attributed to Ta diffusion from the substrate to the surface region during the thermal cycle at a high temperature of ~1450 °C. The Ta diffusion would be more dynamic in the HT-3 sample than in the HT-1 sample because of the higher Ta content in the substrate region. Nevertheless, the outward diffusion of Ta and Hf may be insignificant in both samples considering the slight compositional changes in the samples before and after the thermal cycle. This secures chemical integrity, which is a benefit in the practical use of the material in a sintering crucible.

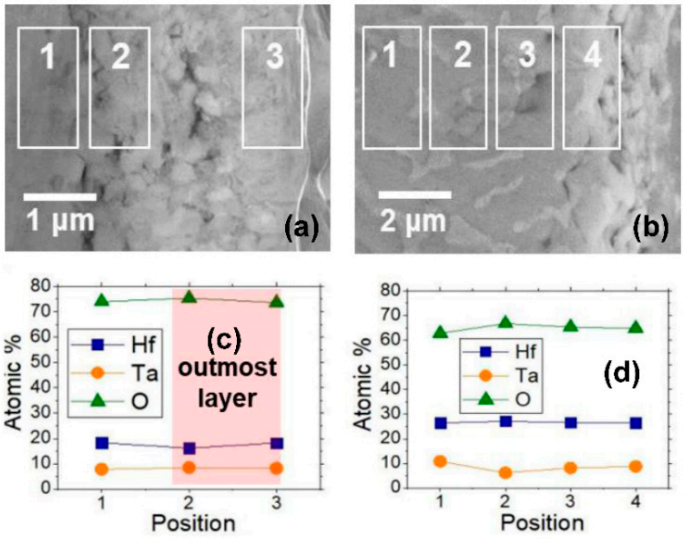

Figure 6. SEM micrographs and EDS results of the (**a**,**c**) HT-1 and (**b**,**d**) HT-3 samples after heat treatment in a 4% H_2-Ar atmosphere.

Figure 7 shows the XRD pattern of the residual powder collected from the HT-3 sample after the thermal cycle. The inset micrographs show changes in the appearance of the samples. Note that only a small amount of residual powder was formed from the HT-1 sample with little change of color. On the other hand, a larger amount of residual powder was observed in the HT-2 and HT-3 samples with significant color changes of the sample surface. In contrast to the HT-2 sample with partial color change, the HT-3 sample color was uniformly white. This color change behavior may be evidence of phase transformation from the original $Hf_6Ta_2O_{17}$ phase to other phases of brighter color. To examine the constituent phases, the residual powder was collected from the HT-3 sample and analyzed by XRD, as shown in Figure 7. The measured pattern reveals that the residual powder contained $Hf_6Ta_2O_{17}$ as a major constituent; that is, the superstructure still remained after the thermal cycle at 1450 °C. However, Hf and Ta were observed as separate phases distinguished by other peaks. This gave evidence of a phase transformation from the Hf-Ta-O superstructure to each separated oxide form, such as Hf-O and Ta-O. The color changes also support this phase separation, considering that the colors of HfO_2 and Ta_2O_5 are bright (e.g., white-like), as revealed in the inset photographs in Figure 7.

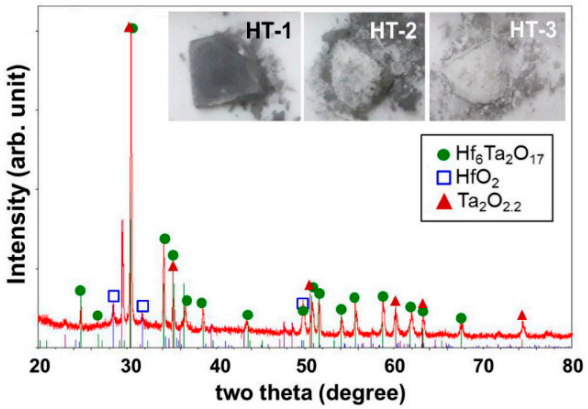

Figure 7. XRD pattern of the residual powder collected from HT-3 after heat treatment in a 4% H_2-Ar atmosphere.

In addition, this phase change would cause the different peeling behaviors of the samples shown in Figures 5 and 6. It is worth noting that the chemical form of Ta oxide is $Ta_2O_{2.2}$ rather than Ta_2O_5,

as presented in the XRD results. This reduction should occur by hydrogen during the thermal cycle. Provided that phase separation occurs from the $Hf_6Ta_2O_{17}$ superstructure, the residual powders are expected to be in the form of HfO_2 and Ta_2O_5. However, in the XRD analysis, the Ta oxide appears to be slightly reduced to $Ta_2O_{2.2}$, while the Hf oxide form is maintained. Due to the lack of thermodynamic information on Ta oxides, it is difficult to precisely calculate the oxygen potential leading to the reduction process. Instead, the observed reduction form empirically shows that the Ta oxide can be reduced under the sintering conditions. More importantly, the reduction of Ta oxide would give rise to breakage of the crystal structure, resulting in the different peeling behavior. The crystal structure of Ta_2O_5 is known to be hexagonal, while $Ta_2O_{2.2}$ is known to be monoclinic [13]. This difference in crystal structure leading to different lattice constants would result in severe lattice distortion and may finally cause destruction of the lattice; i.e., phase-transformation-induced peeling behavior was expected to occur. Accordingly, the amount of reduced Ta oxide affects the degree of lattice distortion; in other words, a higher Ta content facilitates lattice destruction due to reduction. It is therefore expected that the degree of lattice distortion should be mild in the HT-1 sample compared to the distortion in the HT-2 and HT-3 samples. This is supported empirically by the peeling behaviors: note that the outermost layer was maintained at the surface of the HT-1 sample, whereas it peeled off in the HT-2 and HT-3 samples. Based on this, to minimize phase-transformation-induced destruction during thermal cycling in a reducing atmosphere, either the Ta content should be lowered or Ta reduction should be suppressed. As in the case of the sintering in pyroprocessing, if the oxygen potential during thermal cycling is expected to be sufficiently low, resulting in a reduction of Ta oxide into a lower oxidation state (e.g., $Ta_2O_{2.2}$), lowering the initial Ta content should be effective. In this case, the Ta content should be in the range allowing the $Hf_6Ta_2O_{17}$ superstructure to be formed.

4. Conclusions

The $Hf_6Ta_2O_{17}$ superstructure, which is known for its excellent oxidation resistance, was synthesized on the surface of Hf-Ta alloys. The $Hf_6Ta_2O_{17}$ superstructure can have uniform thickness because it originates from a solid/gas reaction at the surface. In order to evaluate its usefulness for a sintering crucible in pyroprocessing, three kinds of Hf-Ta samples with different Ta contents were prepared (HT-1, -2, and -3 with increasing Ta content). The samples were heat treated under the same conditions as those used in the sintering process during the head-end process of pyroprocessing. The samples were then analyzed to evaluate their durability. Only the HT-1 sample with lower Ta content was relatively intact, whereas the HT-2 and HT-3 samples were significantly damaged. From the EDS and XRD results, this difference is ascribed to a reduction of Ta oxide from Ta_2O_5 to $Ta_2O_{2.2}$. The reduction of Ta oxide gave rise to destruction of the crystal structure, manifested as peeling behavior in the HT-2 and HT-3 samples. Accordingly, the degree of damage appears to be magnified by an increase of Ta content. This study therefore demonstrated that lowering the Ta content within the range where the oxidation-resistive superstructure forms is a compositional design strategy that can be exploited to produce a sintering crucible material in pyroprocessing. This result is not limited to pyroprocessing but could also be utilized for other applications of Hf-Ta alloys involving heat treatment in reducing atmospheres.

Funding: This research received no external funding.

Acknowledgments: This work was supported by the National Research Foundation of Korea (NRF) grant funded by the Korea government (Ministry of Education) (No. 2020R1G1A1014475).

Conflicts of Interest: The author declares no conflict of interest.

References

1. Song, K.-C.; Lee, H.-S.; Hur, J.-M.; Kim, J.-G.; Ahn, D.-H.; Cho, Y.-Z. Status of pyroprocessing technology development in Korea. *Nucl. Eng. Technol.* **2010**, *42*, 131–144. [CrossRef]

2. Lee, H.-S.; Park, G.-I.; Kang, K.-H.; Hur, J.-M.; Kim, J.-G.; Ahn, D.-H.; Cho, Y.-Z.; Kim, E.-H. Pyroprocessing technology development at KAERI. *Nucl. Eng. Technol.* **2011**, *43*, 317–328. [CrossRef]
3. Lee, H.; Park, G.-I.; Lee, J.-W.; Kang, K.-H.; Hur, J.-M.; Kim, J.-G.; Paek, S.; Kim, I.-T.; Cho, I.-J. Current Status of Pyroprocessing Development at KAERI. *Sci. Technol. Nucl. Install.* **2013**, *2013*, 343492. [CrossRef]
4. Chang, H.L.; Gao, F.X.; Ko, W.I.; Kim, H.D.; Lee, S.Y. Evaluation of Sigma-MUF (Material Unaccounted For) for the Conceptually Designed Korea Advanced Pyroprocess Facility. *J. Korean Phys. Soc.* **2011**, *59*, 1418–1421. [CrossRef]
5. Sakamura, Y.; Omori, T. Yoshiharu Sakamura Central Research Institute of Electric Power Industry—Iwadokita Komaeshi Tokyo—Japan Electrolytic Reduction and Electrorefining of Uranium to Develop Pyrochemical Reprocessing of Oxide Fuels. *Nucl. Technol.* **2010**, *171*, 266–275. [CrossRef]
6. Choi, E.-Y.; Hur, J.-M.; Choi, I.-K.; Gil Kwon, S.; Kang, D.-S.; Hong, S.S.; Shin, H.-S.; Yoo, M.A.; Jeong, S.M. Electrochemical reduction of porous 17kg uranium oxide pellets by selection of an optimal cathode/anode surface area ratio. *J. Nucl. Mater.* **2011**, *418*, 87–92. [CrossRef]
7. Jeon, S.-C.; Lee, J.-W.; Kang, S.-J.; Lee, J.-H.; Lee, J.-W.; Park, G.-I.; Kim, I.-T. Temperature dependences of the reduction kinetics and densification behavior of U3O8 pellets in Ar atmosphere. *Ceram. Int.* **2015**, *41*, 657–662. [CrossRef]
8. Jeon, S.C.; Lee, J.W.; Yoon, J.Y.; Cho, Y.Z. Scailing up fabrication of UO2 porous pellets with a simulated spent fuel composition. *J. Nucl. Fuel Cycle Waste Technol.* **2017**, *15*, 343–353. [CrossRef]
9. Jeon, S.-C.; Lee, J.-W.; Yoon, J.-Y.; Cho, Y.-Z.; Kim, N.-J.; Kim, D.S.; Kim, K.S.; Kim, J.H.; Yang, J.H. Stimulation of densification during the reduction of U3O8 to UO2 by atmosphere control. *Ceram. Int.* **2019**, *45*, 6863–6868. [CrossRef]
10. Gupta, T.K. Effect of speciment size on the strength degradation of Al2O3 subject to thermal shock. *J. Am. Ceram. Soc.* **1975**, *58*, 158–159. [CrossRef]
11. Spiridonov, F.M.; Mulenkova, M.N. Intermediatephases in the HfO2-Ta2O5 system. *Russ. J. Inorg. Chem.* **1981**, *26*, 922–923.
12. Yang, Y.; Perepezko, J.; Zhang, C. Oxidation synthesis of Hf6Ta2O17 superstructures. *Mater. Chem. Phys.* **2017**, *197*, 154–162. [CrossRef]
13. Donaldson, O.K.; Hattar, K.; Trelewicz, J. Metastable Tantalum Oxide Formation During the Devitrification of Amorphous Tantalum Thin Films. *J. Am. Ceram. Soc.* **2016**, *99*, 3775–3783. [CrossRef]